Non-resonant effects in the $t\bar{t}$ resonance region

Pedro Ruiz-Femenía[1,2] *

1- University of Vienna - Faculty of Physics
Boltzmanngasse 5, A-1090 Wien, Austria

2- Instituto de Física Corpuscular (IFIC), CSIC-Universitat de València
Apdo. Correos 22085, E-46071 Valencia - Spain

The recent developments on the computation of non-resonant corrections to the $e^+e^- \to W^+W^-b\bar{b}$ cross section in the top-antitop resonance region are reviewed in this talk. Non-resonant production of the final state $W^+W^-b\bar{b}$ starts to contribute at NLO in the nonrelativistic power-counting $v \sim \alpha_s \sim \sqrt{\alpha_{\rm EW}}$. The corrections induced by non-resonant effects reduce the cross section in the top-antitop resonance peak region at a level which is comparable to the expected experimental precision at the future linear collider, and are thus relevant for a high-precision top mass and width determination.

1 Introduction

A next generation e^+e^- linear collider such as the International Linear Collider (ILC) operating at energies around the top-antitop threshold will allow us to measure the top-quark's properties with unprecedented precision. The top-quark mass is currently known from direct production at the Fermilab Tevatron (and soon at the Large Hadron Collider) with a precision $\gtrsim$1 GeV. From a threshold scan of the $e^+e^- \to t\bar{t}$ cross section at the ILC, however, an order of magnitude improvement in the precision can be achieved experimentally [1]. Aside from determining a fundamental parameter of the Standard Model, its precise knowledge is important for precision tests of the Standard Model and its extensions. Other characteristics of the top quark such as its width and Yukawa coupling provide information about its coupling to other particles and the mechanism of electroweak symmetry breaking. For these reasons top-quark pair production near threshold in e^+e^- annihilation has been thoroughly investigated following the nonrelativistic QCD (NRQCD) approach, which treats the leading colour-Coulomb force between the nearly on-shell top and antitop exactly to all orders in perturbation theory. In this framework, where the strong coupling α_s is of the same order as v, the small relative velocity of the top and antitop, QCD corrections to the total cross section are known at the next-to-next-to-next-to-leading order (NNNLO) [2–4], and higher-order logarithms $(\alpha_s \log v)^k$ have been resumed to next-to-next-to-leading logarithmic order (NNLL) [5]. The NNLL prediction, which had a normalization uncertainty in the total cross section $\gtrsim 6\%$, has been recently updated [6], showing a substantial reduction of the renormalization scale dependence. An analysis collecting all the pieces that contribute to the full NNNLO total cross section is still pending (see [3] for the latest summary), which would provide information about the convergence of the non-logarithmic piece of the QCD corrections.

Here we focus on subleading corrections of electroweak origin. The top quark is unstable with a significant width Γ_t of about 1.5 GeV due to the electroweak interaction. Once the top width is included, due to top decay, the physical final state is $W^+W^-b\bar{b}$ – at

*Talk based on work done in collaboration with A. Hoang and C. Reisser, and on work done in collaboration with M. Beneke and B. Jantzen. Preprint numbers: UWThPh-2012-10, IFIC/12-12.

least if we neglect the decay of top into strange and down quarks, as justified by $V_{tb} \approx 1$, and consider W bosons as stable. The $W^+W^-b\bar{b}$ final state can also be produced non-resonantly, *i.e.* through processes which do not involve a nearly on-shell $t\bar{t}$ pair. The latter effects are not included in the standard nonrelativistic treatment used to compute the dominant QCD corrections, which can only describe the resonant process with a nearly on-shell $t\bar{t}$ intermediate state, but can be accommodated using the effective field theory (EFT) formalism to describe pair production of unstable particles at threshold [7–9]. Adopting a counting scheme where $\alpha_{\rm EW} \sim \alpha_s^2$, the leading non-resonant and off-shell effects are NLO for the total cross section, since there is an additional power of $\alpha_{\rm EW}$ but no phase space suppression, hence the relative correction is $\alpha_{\rm EW}/v \sim \alpha_s$. At NLO they can be classified as part of the electroweak corrections to the $e^+e^- \to W^+W^-b\bar{b}$ cross section, and are dominant compared to the purely resonant electroweak effects, which first contribute at NNLO [9]. The identification of non-resonant production of the final state $W^+W^-b\bar{b}$ as a pure electroweak effect does not hold anymore at NNLO, where gluon corrections to the non-resonant part have to be considered.

In this talk I discuss the status of the calculation of the non-resonant contributions to the $e^+e^- \to W^+W^-b\bar{b}$ process in the $t\bar{t}$ resonance region. The results at NLO are fully known for the total cross section as well as including invariant-mass cuts on the Wb pairs. At NNLO, interesting conceptual issues regarding the interplay between resonant and non-resonant parts of the calculation arise. These are discussed in Sec. 3. The computation of the full set of NNLO non-resonant corrections represents a much more difficult task that has not yet been attempted. An alternative approach, named "NRQCD phase space matching", to compute the non-resonant effects beyond NLO entirely through calculations in NRQCD has been proposed [10, 11], which works if moderate invariant-mass cuts on the Wb pairs are applied. The concepts of the phase space matching and the results from this method are reviewed in the last section.

2 Non-resonant NLO electroweak contributions

The cross section for the $e^+e^- \to W^+W^-b\bar{b}$ process is obtained from the $W^+bW^-\bar{b}$ cuts of the e^+e^- forward-scattering amplitude. In the energy region $\sqrt{s} \approx 2m_t$ the amplitude is dominated by the production of resonant top quarks with small virtuality. A separation of resonant and non-resonant effects can be consistently achieved within the unstable-particle effective field theory [7]. This allows us to integrate out hard modes ($\sim m_t$) and represent the forward-scattering amplitude as the sum of two terms,

$$\begin{aligned} i\mathcal{A} &= \sum_{k,l} C_p^{(k)} C_p^{(l)} \int d^4x \, \langle e^-e^+|\mathrm{T}[i\mathcal{O}_p^{(k)\dagger}(0)\, i\mathcal{O}_p^{(l)}(x)]|e^-e^+\rangle \\ &\quad + \sum_k C_{4e}^{(k)} \langle e^-e^+|i\mathcal{O}_{4e}^{(k)}(0)|e^-e^+\rangle. \end{aligned} \tag{1}$$

The matrix elements in (1) are evaluated in the "low-energy" effective theory, which includes elements of soft-collinear and nonrelativistic effective theory. The first term on the right-hand side of (1) describes the production of a resonant $t\bar{t}$ pair in terms of production (decay) operators $\mathcal{O}_p^{(l)}(x)$ ($\mathcal{O}_p^{(k)\dagger}(x)$) with short-distance coefficients $C_p^{(k,l)}$. The second term accounts for the remaining non-resonant contributions, which in the effective theory are

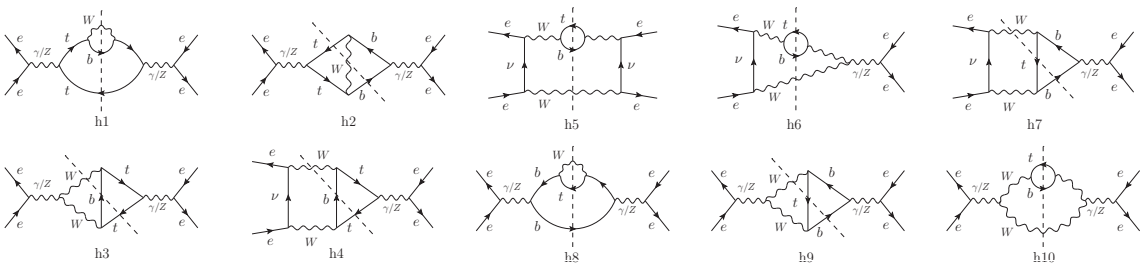

Figure 1: Two-loop forward-scattering amplitude diagrams with $\bar{t}bW^+$ cuts. $t\bar{b}W^-$ cuts and symmetric diagrams are not shown.

described by four-electron production-decay operators $\mathcal{O}_{4e}^{(k)}$. The coefficients $C_{4e}^{(k)}$ originate from the hard contributions of the e^+e^- forward-scattering amplitude. The hard momentum region expansion dictates that the top-quark self-energy insertions are treated perturbatively, since the top lines are formally far off-shell, $p_t^2 - m_t^2 \sim \mathcal{O}(m_t^2) \gg \Sigma(p_t^2)$. Accordingly the calculation of the coefficients $C_{4e}^{(k)}$ is performed in fixed-order perturbation theory in the full electroweak theory with no resummation of self-energy insertions in the top-quark propagator [8] and supplemented with an expansion of the amplitudes near threshold (in $\delta = s/(4m_t^2) - 1 \sim v^2$). The leading imaginary parts of $C_{4e}^{(k)}$ arise from the cut two-loop diagrams of order $\alpha_{\rm EW}^3$ shown in Fig. 1. The corresponding contribution to the cross section is

$$\sigma_{\rm non-res} = \frac{1}{s} \sum_k \mathrm{Im}\left[C_{4e}^{(k)}\right] \langle e^-e^+|i\mathcal{O}_{4e}^{(k)}(0)|e^-e^+\rangle. \tag{2}$$

Technically, this simply amounts to the calculation of the spin-averaged tree-level processes $e^+e^- \to tW^-\bar{b}$ and $e^+e^- \to \bar{t}W^+b$ with no width supplied to the intermediate top-quark propagators. Instead, the divergence from the top-quark propagators going on-shell is regularized dimensionally. Details on the computation and integral representations of the result for (2) can be found in [12]. The results of [12] for the NLO non-resonant contribution to the total cross section have been confirmed recently by an independent calculation [13]. The latter is based on an expansion in the parameter $\rho = 1 - M_W/m_t \approx 0.53$, which for individual diagrams requires to consider several orders in ρ or to use Padé approximants to reach a precise numerical agreement with the integral representation of [12]. For the sum of all diagrams, however, the leading order in ρ gives an approximation which differs from the exact result by less than 5%.

Through the computation of the four-electron matching coefficients loose cuts ($\sim m_t$) on the bW^+ and $\bar{b}W^-$ invariant masses can be incorporated easily, as it has been discussed in the context of W-pair production near threshold [14]. The result obtained in [12] covers the case of symmetric cuts on the invariant mass of the bW subsystems (p_{bW}^2) of the form

$$m_t - \Delta M_t \le \sqrt{p_{bW}^2} \le m_t + \Delta M_t\,, \tag{3}$$

for $\Delta M_t \gg \Gamma_t$, up to the total cross section ($\Delta M_{t,\rm max} = m_t - M_W$).

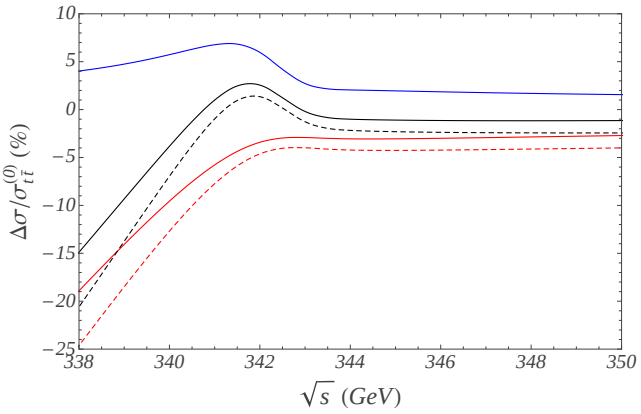

Figure 2: Relative sizes of the QED and non-resonant corrections with respect the $t\bar{t}$ LO cross section in percent: $\sigma^{(1)}_{\rm QED}/\sigma^{(0)}_{t\bar{t}}$ (upper solid blue line), $\sigma^{(1)}_{\text{non-res}}/\sigma^{(0)}_{t\bar{t}}$ for the total cross section (lower solid red line) and $\Delta M_t = 15$ GeV (lower dashed red line). The relative size of the sum of the QED and non-resonant corrections is represented by the middle lines, for $\Delta M_{t,\rm max}$ (solid) and $\Delta M_t = 15$ GeV (dashed). We have chosen $\alpha_s(30\,\text{GeV}) = 0.142$ and $m_t = 172$ GeV.

2.1 Results

The plot in Fig. 2 displays the relative sizes of the NLO electroweak corrections with respect to the LO result for the $e^+e^- \to W^+W^-b\bar{b}$ cross section, which includes the summation of Coulomb corrections. The QED contribution represents a correction of about 2% above threshold and rises to a maximum of 7% just below the peak, while the non-resonant contributions give a constant negative shift of about 3% above threshold. Below threshold the relative size of the non-resonant corrections is very large, since the LO result rapidly vanishes, reaching up to 19%. Hence below threshold they represent the leading electroweak correction to the total $t\bar{t}$ cross section. We observe a partial cancellation of the QED and non-resonant corrections in the peak region and at energies above. A sensitivity to the invariant-mass cut ΔM_t in the bW^+ and $\bar{b}W^-$ subsystem enters first at NLO through the non-resonant contributions. Restricting the available phase space for the final-state particles by tightening the invariant-mass cuts ΔM_t makes the non-resonant contributions even more important. This is shown by the dashed lines in Fig. 2, corresponding to $\Delta M_t = 15$ GeV. The non-resonant correction amounts to a negative shift of 27–35 fb for $\sqrt{s}$ in the interval $(338, 350)$ GeV.

3 Non-resonant effects beyond NLO

3.1 Finite-width divergences

There is an interesting conceptual issue concerning the resonant part of the QCD calculation of the $t\bar{t}$ cross section. At NNLO it exhibits an uncanceled ultraviolet divergence (here

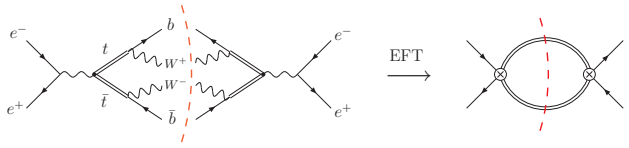

Figure 3: Tree-level double-resonant diagrams in the full and effective theories. Double lines are used for representing top quarks. The (red) dashed line denotes that we extract the imaginary part of the forward scattering amplitude or, equivalently, that we perform the phase space integration over the particles in the cut.

regulated dimensionally)

$$\sigma_{t\bar{t}} \propto \frac{\alpha_s \Gamma_t}{\epsilon} \propto \frac{\alpha_s \alpha_{\rm EW}}{\epsilon}\,, \tag{4}$$

which arises from the logarithmic overall divergence in the two-loop nonrelativistic correlation function, whose imaginary part gives the cross section. The overall divergence is polynomial in the nonrelativistic energy E of the top quarks, but contributes to the cross section if $\Gamma_t \neq 0$, since the correlation function is evaluated at complex values $E \to E + i\Gamma_t$. It can be shown that these UV-divergences originate because the unstable particle propagators describing the top and antitop in the EFT allow for contributions to the forward scattering amplitude from intermediate states which have arbitrarily large invariant masses.

The inclusion of a finite width in the top propagator changes the high-energy behaviour of its imaginary part and makes the phase space integration extend to infinity. To illustrate the latter consider the Born cross section diagram in the EFT, Fig. 3. The cutting rules for the top lines imply extracting the real part of the NRQCD propagator: in the stable case ($i\Gamma_t/2 \to i\epsilon$) we have

$$\mathrm{Re}\left[\frac{i}{p_0 - \frac{\mathbf{p}^2}{2m_t} + i\epsilon}\right] = \pi\,\delta\Big(p^0 - \frac{\mathbf{p}^2}{2m_t}\Big)\,, \tag{5}$$

which imposes a fixed dispersion relation $p^0 = \mathbf{p}^2/2m_t$, while the real part of the unstable propagator,

$$\mathrm{Re}\left[\frac{i}{p_0 - \frac{\mathbf{p}^2}{2m_t} + i\frac{\Gamma_t}{2}}\right] = \frac{\Gamma_t/2}{(p_0 - \frac{\mathbf{p}^2}{2m_t})^2 + (\frac{\Gamma_t}{2})^2}\,, \tag{6}$$

yields a Breit-Wigner distribution with support in the entire $(p^0, |\mathbf{p}|)$ plane.

From the point of view of the full theory, already taking the nonrelativistic limit makes the phase space integration extend to infinity. Consider the full-theory double-resonant diagram of Fig. 3 with center-of-mass momentum $q = (2m_t + E, \mathbf{0})$. When the quark lines are close to their mass shell the 4-particle phase space integration reduces to

$$\sigma_{t\bar{t}} \sim \int_{-\infty}^{+\infty} dp_0 \int_0^{+\infty} d|\mathbf{p}|\mathbf{p}^2 \frac{\Gamma_t^2}{\left|m_t E + 2m_t p_0 - \mathbf{p}^2 + i\epsilon\right|^2 \left|m_t E - 2m_t p_0 - \mathbf{p}^2 + i\epsilon\right|^2}\,, \tag{7}$$

where in the denominator we have retained the leading order term in the nonrelativistic expansion of the top and antitop off-shellness, $(p_{t,\bar{t}}^2 - m_t^2)$, with $p_{t,\bar{t}}^2 = (q/2 \pm p)^2$. The Γ_t^2 factor in the numerator arises from the phase space integration of the bW^+ and $\bar{b}W^-$

subsystems because in the nonrelativistic limit the top and antitop quark are effectively on-shell. We notice that the integration limits in Eq. (7), which in the full theory computation are cut off by the top mass, become infinite in the nonrelativistic limit. The boundaries of the phase space are determined by step functions in the phase space measure, and the arguments of these functions also have to be expanded according to the nonrelativistic power-counting. In the limit $m_t \gg (p^0, |\mathbf{p}|)$ the step functions do not depend on $(p^0, |\mathbf{p}|)$ any longer, and are satisfied trivially, thus allowing for an infinite integration region in these variables. The corresponding NRQCD amplitude (diagram on the right in Fig. 3) reproduces Eq. (7) when Γ_t is treated as an insertion. The NRQCD power-counting, however, tells that the $\Gamma_t \sim E$ term needs to be resummed as part of the top propagator, thus effectively replacing $i\epsilon$ by a term proportional to $i\Gamma_t$ as in Eq. (6).

Despite the integration limits, the tree-level integration in Eq. (7) is finite. However the integrand becomes more sensitive to large momentum regions once we include relativistic corrections $\sim \mathbf{p}^2/m_t^2$. Using dimensional regularization these subleading contributions can lead to $1/\epsilon$ singularities if the high energy behaviour of the EFT phase space integration is logarithmic. The lesson from this is that the pure resonant result alone that is usually shown in the literature is inconsistent theoretically and must be supplemented with additional short-distance information from the systematic calculation of the $e^+e^- \to W^+W^-b\bar{b}$ process.

3.2 Towards an evaluation of the NNLO non-resonant contributions

Since the full-theory calculation is finite, the UV divergence in the NNLO resonant part must cancel with an infrared divergence that appears in the non-resonant term in unstable-particle effective theory from diagrams corresponding to off-shell top-quark decay, as discussed in [4]. The NNLO contributions to $\sigma_{\rm non-res}$ are given by the $\mathcal{O}(\alpha_s)$ corrections to the diagrams h_{1-10} in Fig. 1 (an example is provided by Fig. 4). Parts of the latter consist of gluon radiation diagrams, which thus contribute first at NNLO in the non-resonant part, in contrast to what happens in the resonant part, where ultrasoft gluon radiation is a N^{3}LO effect.

Divergences in the non-resonant part arise when the top (or antitop) propagators go on-shell [12]. This is a consequence of the hard momentum region expansion, which sets $\Gamma_t = 0$ in the top-antitop propagators and forces to retain the leading order term of the upper kinematic limit in $p_t^2 \equiv p_{bW}^2$: $p_{t,\rm max}^2 = m_t^2 + \mathcal{O}(\delta)$. Integrating over all other kinematic variables but p_t^2, the non-resonant contributions involve integrals of the form

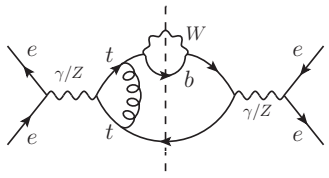

Figure 4: NNLO contribution to $\sigma_{\rm non-res}$

$$\int_{p_{t,\rm min}^2}^{m_t^2} \frac{dp_t^2}{(m_t^2 - p_t^2)^{n+a\epsilon}} = \frac{1}{1-n-a\epsilon} \, (m_t^2 - p_{t,\rm min}^2)^{1-n-a\epsilon} \,, \tag{8}$$

where the endpoint singularity at $p_t^2 = m_t^2$ is regularized in $d = 4 - 2\epsilon$ dimensions. At NLO, only the diagram h_1 has an endpoint divergence, with $n = 3/2$, and the result is therefore finite in the limit $\epsilon \to 0$. Gluon corrections, on the other hand, yield additional half-integer powers of $(m_t^2 - p_t^2)$ and, in particular, $n = 1$ contributions which will generate $1/\epsilon$ terms of the form (4). For example, the gluon vertex correction to diagram h_1 shown in Fig. 4

yields non-zero contributions with $n = 2, \frac{3}{2}, 1, \frac{1}{2}, \ldots$, and one can check that the resulting divergences cancel those in the resonant part of the full-theory diagram. Clearly, the complexity associated with the evaluation of the full NNLO set of non-resonant corrections calls for a numerical implementation using Monte Carlo methods for the phase space integration. Such an implementation requires that the end-point divergences occurring in the diagrams are identified and subtracted from the amplitude, together with the soft-collinear divergences that show up at NNLO due to gluon radiation. The complete set of NNLO non-resonant singularities shall be available soon [15].

It should be mentioned that the leading term of the expansion in $\rho = 1 - M_W/m_t$ of the NNLO non-resonant contribution to the total cross section has been given in Ref. [13]. The accuracy of such an approximation, though, cannot be estimated reliably without further knowledge of the size of subleading terms in the ρ-expansion.

4 Phase space matching

An alternative approach to account for non-resonant effects has been developed in parallel [10, 11] that includes the effects of invariant-mass cuts on the Wb pairs entirely through calculations in an extended version of NRQCD which accounts for unstable particle effects systematically [9]. In this approach, the UV-divergences from the resonant matrix elements are compensated by imaginary counter-terms associated with the $(e^+e^-)(e^+e^-)$ forward-scattering operators, which thus acquire an imaginary anomalous dimension and sum large logarithms of the top velocity. In Ref. [11] we demonstrate that for moderate top invariant mass cuts of the form (3) with $\Delta M_t \sim 15 - 35$ GeV, the matching conditions of the $(e^+e^-)(e^+e^-)$ forward scattering operators are dominated by the NRQCD phase space contributions, i.e. they can be computed from the difference between the (potentially) divergent NRQCD phase space integrations without any cuts and the ones with the cuts in Eq. (3) being imposed. This is because using the $\overline{\rm MS}$ scheme in NRQCD diagrams involving the unstable top propagator of Eq. (6) largely overestimates the contributions from unphysical phase space regions that are parametrically away from the potential, soft and ultrasoft regions that can be described by NRQCD. Thus the main numerical effect of the "phase space matching" procedure is obtained by removing these unphysical contributions and can be carried out within NRQCD itself.

An important conceptual aspect of the invariant mass cuts defined in Eq. (3) is that already for moderate cuts $\Delta M_t \sim 15 - 35$ GeV the cut $\Delta\mathbf{p}$ on the nonrelativistic (anti)top three-momentum $\mathbf{p}$ is $\Delta\mathbf{p} \sim \sqrt{2m_t\Delta M_t} \sim 100$ GeV, and thus represents a hard scale of the order m_t. This justifies the implementation of the phase space effects into the matching conditions of the Wilson coefficients. Since $\Lambda \equiv \sqrt{2m_t\Delta M_t}$ is parametrically of order m_t we use for our bookkeeping the counting $\Lambda \sim m_t$. In this counting scheme the phase space constraints are incorporated through the NRQCD Wilson coefficients. On the other hand, numerically the scales ΔM_t and Λ are sufficiently below the top mass scale such that all $t\bar{t}$ phase space configurations that pass the invariant mass constraint can still be adequately described by NRQCD. This fact is crucial for the phase space matching method briefly outlined in the following.

Consider first the case without QCD effects ($\alpha_s = 0$). For the determination of the Wilson coefficients $\tilde{C}^{(n)}_{V/A}$ we need to know the result for the inclusive cross section $\sigma^{\alpha_s=0}_{\rm incl}(\Lambda)$ with

invariant mass constraints [a]. In the common approach to matching computations, $\sigma_{\rm incl}^{\alpha_s=0}(\Lambda)$ is computed in the full relativistic theory. After the result is expanded nonrelativistically using the counting $v \sim \sqrt{\alpha_{\rm EW}}$, one can identify the pieces belonging to the Wilson coefficients $\tilde{C}_{V/A}^{(n)}$. On the other hand, as mentioned above, the $t\bar{t}$ phase space regions passing the invariant mass cuts can be determined within the nonrelativistic expansion. We therefore write the expression for the inclusive cross section as a sum of two terms,

$$\sigma_{\rm incl}^{\alpha_s=0}(\Lambda) \;=\; \sigma_{\rm NRQCD}^{\alpha_s=0}(\Lambda) + \sigma_{\rm rem}^{\alpha_s=0}(\Lambda)\,. \tag{9}$$

Here, $\sigma_{\rm NRQCD}^{\alpha_s=0}$ is the cross section computed from NRQCD Feynman rules with the (anti)top invariant mass constraints being applied for the phase space integration. The parameter Λ is related to the invariant mass cut ΔM_t and we use the formal counting $\Lambda \sim m_t$ according to the discussion above. In this computation the $(e^+e^-)(e^+e^-)$ forward scattering operators do not contribute, and the resulting expressions are just the nonrelativistic expansions of full theory squared matrix elements containing the square of the double resonant diagram $e^+e^- \to t\bar{t} \to W^+W^-b\bar{b}$ (see Fig. 5a) and the interference of the double resonant diagram with the diagrams for $e^+e^- \to W^+W^-b\bar{b}$ having only either the top or the antitop in intermediate stages (see Fig. 5b and c for typical diagrams). The contributions to the Wilson coefficients $\tilde{C}_{V/A}^{(n)}$ that result from $\sigma_{\rm NRQCD}^{\alpha_s=0}(\Lambda)$ are local (i.e. energy-independent) and have the form

$$\frac{\Gamma_t}{\Lambda} \sum_{n,k=0} \left[\left(\frac{m_t\Gamma_t}{\Lambda^2} \right)^n \times \left(\frac{\Lambda^2}{m_t^2} \right)^k \right], \tag{10}$$

where the first term in the expansion, proportional to Γ_t/Λ, arises from the leading order diagram for the phase space matching computation (right diagram in Fig. 3) and gives the dominant phase space correction to the $t\bar{t}$ cross section. In the counting $\Lambda \sim m_t$, it constitutes an $\mathcal{O}(v^2)$ correction (NLL[b]), since $\Gamma_t/m_t \sim v^2$. The Λ^2/m_t^2 terms arise from insertions of operators that are higher order in the nonrelativistic expansion, and since they are formally of order unity, can lead to power-counting breaking contributions. However, we find that the numerical effects of the power-counting breaking contributions are very small and do not spoil the nonrelativistic expansion. This is partly due to the fact that the phase space cutoff Λ is sufficiently smaller than the convergence radius of the nonrelativistic expansion. The phase space matching procedure can thus be implemented for values of the invariant mass cut in the range $m_t\Gamma_t \ll \Lambda^2 \lesssim m_t^2$, but not for the total cross section where Λ is numerically of order m_t.

The remainder contribution of the inclusive cross section, $\sigma_{\rm rem}^{\alpha_s=0}(\Lambda)$ accounts for all other contributions to the full theory matrix element. This includes for example pure background $e^+e^- \to W^+W^-b\bar{b}$ diagrams, see Fig. 5d for a typical diagram, and also the square of the single-top diagrams in Figs. 5b and c. One can check that the first two terms in the phase space matching series (10) agree with the two first terms in the expansion in Λ^2/m_t^2 of the full NLO non-resonant result. This means that the remainder contributions, not calculable

[a] The Wilson coefficients $\tilde{C}_{V/A}^{(n)}$ correspond to the $C_{4e}^{(k)}$ coefficients of Eq. (1), following the notation of [11], which is explained in their Sec. II.

[b] In the NRQCD approach were logarithms are summed systematically the counting LO, NLO... is replaced by leading logarithmic (LL) order, next-to-leading logarithmic (NNL) order and so on.

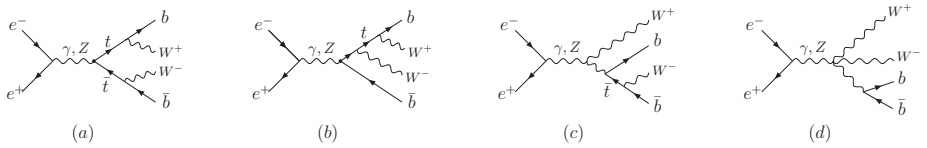

Figure 5: (a) Full theory diagram for $e^+e^- \to t\bar{t} \to W^+W^-b\bar{b}$. (b,c) Typical single-resonant full theory diagram for $e^+e^- \to W^-t\bar{b} \to W^+W^-b\bar{b}$. (d) Typical full theory diagram for $e^+e^- \to W^+W^-b\bar{b}$ without top or antitop quarks as intermediate states.

within the phase space matching approach, first contribute with $\Gamma_t\Lambda^3/m_t^4$ terms, and should therefore be small for the range of Λ used in [11]. Indeed, the remainder contribution was determined in [11] by computing the full $e^+e^- \to W^+W^-b\bar{b}$ cross section at tree-level with MadGraph, and shown to be smaller than 5 fb; it can thus be neglected in view of the expected experimental precision expected at a future linear collider. Since no kinematic or dynamical enhancement is expected for the QCD corrections to the remainder contributions, we assume these are also negligible when $\alpha_s \neq 0$. This simplifies the computations substantially and makes the determination of higher order QCD corrections feasible in the phase space matching approach. A calculation of the full NNLO non-resonant contributions along the lines of Sec. 3.2 shall confirm this assumption.

The QCD corrections introduce powers of $(\alpha_s m_t/\Lambda)$ in the phase space matching series (10). As far as the α_s-expansion is concerned, we have found that the N^{3}LL ($\mathcal{O}(\alpha_s^2)$) corrections to the phase space matching contributions need to be determined to meet the experimental precision expected at a future linear collider. An important part of these N^{3}LL corrections have been computed analytically in [11], together with the complete set of NLL and NNLL ones. It is interesting to note that at N^{3}LL order one has to include also the phase space matching for $(e^+e^-)(t\bar{t})$ top production operators. This is because at higher orders in the loop expansion, one has to account for the phase space matching contributions of subdiagrams to remove non-analytic matrix element terms from the matching equations and to achieve that the matching coefficients are analytic in the external energy. The procedure of carrying out the phase space matching is thus analogous to the common matching and renormalization methods for stable particle theories.

4.1 Results

In Fig. 6 we show the phase space matching corrections to the inclusive $t\bar{t}$ threshold cross section up to N^{3}LL order, for invariant mass cuts of $\Delta M_t = 15$ GeV and $\Delta M_t = 35$ GeV, and compare them with the rest of electroweak corrections. The QED effects arise from the electromagnetic correction to the QCD Coulomb potential and the one-loop QED matching correction to the Wilson coefficient of the $t\bar{t}$ current. The hard one-loop electroweak corrections have been obtained in Ref. [16]. The type-1 finite lifetime corrections represent all finite lifetime corrections which are not related to phase space constraints. They consist of the corrections generated by the imaginary interference matching coefficient, the time dilation corrections to the Green function, both known at NNLL order, and the contributions from the renormalization group summation of the NLL phase space logarithms [9]. The QED, hard electroweak and type-1 finite lifetime corrections do not depend on phase

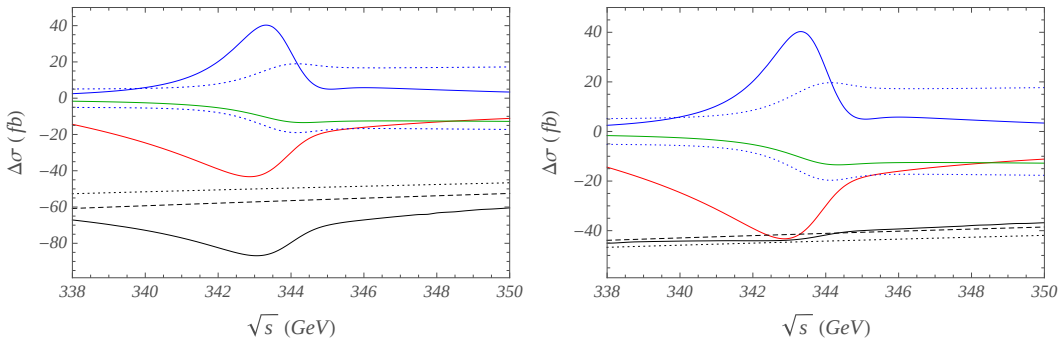

Figure 6: Sizes of the different contributions to the inclusive cross section arising from electroweak interactions as a function of the total c.o.m energy for $\Delta M_t = 15$ GeV (left) and $\Delta M_t = 35$ GeV (right): (green line) NNLL hard one-loop electroweak effects from Ref. [16], (red line) NNLL finite lifetime corrections from Ref. [9], (blue line) NNLL QED effects, and phase space matching corrections at NLL, NNLL and N^{3}LL (dotted, dashed and solid black lines, respectively). The blue dotted lines correspond to the expected experimental uncertainties at the LC. The values used for input parameters are those of Ref. [11].

space restrictions and are therefore identical in both panels. In Fig. 6 the blue dotted lines represent a rough estimation of the expected experimental uncertainties at a future linear collider consisting of an energy-independent error of 5 fb and a 2% relative uncertainty with respect to the full prediction, both being added quadratically.

We see that the QED (blue lines) and the type-1 finite lifetime corrections (red lines) are sizeable (at the level of 40 fb) only in the peak region just below $\sqrt{s} = 2m_t$. Due to their different signs the QED corrections and the type-1 finite lifetime corrections cancel each other to a large extent in the peak region. The hard electroweak corrections (green lines) represent a multiplicative factor of -1.2% to the total cross section and are therefore very small below the peak and at the level of 12-13 fb above the peak region. We see that the phase space matching contributions represent the largest of the four classes of electroweak effects. In contrast to the other classes of electroweak effects they do not decrease strongly for energies below the peak region. For $\Delta M_t = 15$ GeV the N^{3}LL phase space matching contributions amount between -85 and -65 fb and for $\Delta M_t = 35$ GeV they are between -45 and -35 fb. The overall size of the phase space matching corrections decreases for larger values of the top invariant mass cut ΔM_t. We emphasize, however, that the results obtained within the phase space matching approach are valid only for moderate values of ΔM_t in the region between 15 and 35 GeV. For invariant mass cuts below 15 GeV the phase space constraints are not related anymore to hard effects and for invariant mass cuts substantially above 35 GeV matching contributions that need to be computed from full theory diagrams have to be included. The relatively flat behavior of the phase space matching contributions is related to the fact that the dominant phase space matching contributions are energy-independent. The small linear dependence on $\sqrt{s}$ is related to the $\sqrt{s}$ dependence of the virtual γ and Z propagators of the basic $e^+e^- \to t\bar{t}$ process and the peak-like structure comes from an imaginary phase space matching contribution to the $(e^+e^-)(t\bar{t})$ top pair production operator which enters the N^{3}LL inclusive cross section in terms of a time-ordered product.

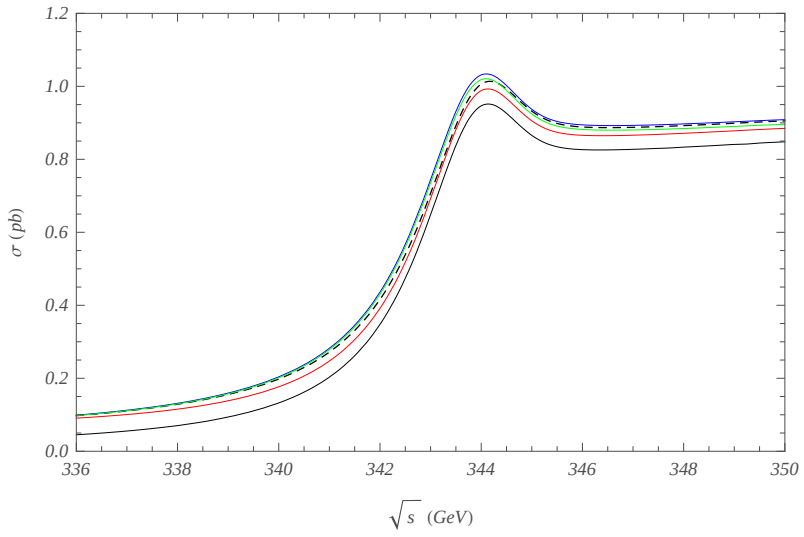

Figure 7: Total inclusive top pair production cross section from NRQCD: starting from the pure QCD NNLL prediction (black dashed line), we add step-by-step the QED corrections (blue line), the hard electroweak corrections (green line), the type-1 finite lifetime corrections (red line) and the N^{3}LL phase space corrections (black solid line) for $\Delta M_t = 35$ GeV.

The results for the NLL, NNLL and N^{3}LL phase space marching contributions displayed in Fig. 6 show that the expansion related to the phase space matching procedure is particularly good for larger values of ΔM_t and still well under control for $\Delta M_t = 15$ GeV. We note that the rather small size of the NNLL corrections (difference of black dotted and dashed lines) for $\Delta M_t = 15$ GeV arises from a cancellation between different independent NNLL corrections.

In Fig. 7 the size of the four different types of electroweak corrections is shown for predictions of the total inclusive cross section for $\Delta M_t = 35$ GeV. We again see that the phase space matching contributions exceed by far the other electroweak corrections. The phase space matching contributions are between -85 and -35 fb for invariant mass cuts ΔM_t between 15 and 35 GeV and are essential for realistic theoretical predictions. In the peak and the continuum region ($\sqrt{s} \gtrsim 2m_t$) they amount to 6 to 10%. They are particularly important in the region below the peak ($\sqrt{s} \lesssim 2m_t$) where the cross section decreases and the unphysical off-shell contributions of the NRQCD $t\bar{t}$ phase space become dominant. Here the phase space matching contributions can amount to more than 50%, and they ensure that the cross section has the correct physical behavior.

5 Acknowledgments

I would like to thank the organizers for the excellent workshop and hospitality. I also thank B. Jantzen for comments on the manuscript. This work is partly supported by the grant FPA2007-60323 and by the Spanish Consolider-Ingenio 2010 Programme CPAN (CSD2007-00042).

References

[1] M. Martinez and R. Miquel, Eur. Phys. J. **C27**, 49 (2003).

[2] M. Beneke, Y. Kiyo and K. Schuller, Nucl. Phys. **B714**, 67 (2005).

[3] M. Beneke, Y. Kiyo and K. Schuller, PoS **RADCOR2007**, 051 (2007).

[4] M. Beneke and Y. Kiyo, Phys. Lett. **B668**, 143 (2008).

[5] A. H. Hoang, A. V. Manohar, I. W. Stewart and T. Teubner, Phys. Rev. Lett. **86**, 1951 (2001); A. H. Hoang, A. V. Manohar, I. W. Stewart and T. Teubner, Phys. Rev. **D65**, 014014 (2002); A. Pineda and A. Signer, Nucl. Phys. **B762**, 67 (2007).

[6] A. Hoang and M. Stahlhofen, arXiv:1111.4486 [hep-ph].

[7] M. Beneke, A. P. Chapovsky, A. Signer and G. Zanderighi, Phys. Rev. Lett. **93**, 011602 (2004); M. Beneke, A. P. Chapovsky, A. Signer and G. Zanderighi, Nucl. Phys. **B686**, 205 (2004).

[8] M. Beneke, P. Falgari, C. Schwinn, A. Signer and G. Zanderighi, Nucl. Phys. **B792**, 89 (2008).

[9] A. H. Hoang and C. J. Reisser, Phys. Rev. **D71** (2005) 074022.

[10] A. H. Hoang, C. J. Reisser and P. Ruiz-Femenia, Nucl. Phys. Proc. Suppl. **186**, 403 (2009).

[11] A. H. Hoang, C. J. Reisser and P. Ruiz-Femenia, Phys. Rev. **D82**, 014005 (2010).

[12] M. Beneke, B. Jantzen and P. Ruiz-Femenia, Nucl. Phys. **B840**, 186 (2010).

[13] A. A. Penin and J. H. Piclum, JHEP **1201** (2012) 034.

[14] S. Actis, M. Beneke, P. Falgari and C. Schwinn, Nucl. Phys. **B807**, 1 (2009).

[15] B. Jantzen and P. Ruiz-Femenia, work in preparation.

[16] A. Hoang and C. Reisser, Phys. Rev. **D74** (2006) 034002.